Energetic perspective on the crystal structure organization principles of meta-halogen-substituted anilines

Irina S. Konovalova, Nils Nöthling, Guido J. Reiss

Article - Version of Record

Journal of Molecular Structure 1349 (2026) 143745

Contents lists available at ScienceDirect

Journal of Molecular Structure

journal homepage: www.elsevier.com/locate/molstr

Energetic perspective on the crystal structure organization principles of *meta*-halogen-substituted anilines

Irina S. Konovalova [a,b,*], Nils Nöthling [c], Guido J. Reiss [b]

[a] SSI "Institute for Single Crystals", National Academy of Science of Ukraine, 60 Nauky ave., Kharkiv, 61001, Ukraine
[b] Institut fur Bioanorganische Chemie Heinrich-Heine-Universitat Dusseldorf, Universitatsstrasse 1 40225 Dusseldorf, Germany
[c] Max-Planck-Institut für Kohlenforschung, Kaiser-Wilhelm-Platz 1 45470 Mülheim an der Ruhr, Germany.

ARTICLE INFO

Keywords:
Halogen bond
Hydrogen bond
haloaniline
Crystal packing analysis
Interaction energy
Capillary crystallisation

ABSTRACT

The crystal structures of *meta*-halogenated anilines 3-chloro- and 3-bromaniline have been determined for the first time. The crystal structure 3-iodoanoiline was re-determined with a sufficient quality using single-crystal X-ray diffraction. All three structures were analyzed from both geometric and energetic perspectives. Geometric analysis reveals common motifs such as zig-zag chains, bifurcated halogen bonds, and the dual donor–acceptor role of amino groups in hydrogen bonding. An energy-based approach, utilizing quantum chemical calculations, enables identification of the dominant interactions and basic structural motifs. While 3-chloroaniline forms columnar structures dominated by N–H···N and C–H···π interactions, the bromo- and iodo-analogs exhibit isostructural columnar-layered packing motives governed by stronger halogen bonding and π-type interactions. This combined approach emphasizes the importance of energy analysis in distinguishing structural hierarchies in systems with multiple weak interactions.

1. Introduction

Haloanilines belong to a well-known class of organic compounds derived from aniline. The introduction of halogen atoms onto the aniline scaffold is crucial for the corresponding reactivity and some physicochemical properties. In detail, the halogen-substitution modifies the compound's acidity/basicity, polarity, solubility and reactivity in general. Halogen-substituted anilines have been in the focus of extensive scientific investigation, with several hundred studies dedicated to their analysis [1–6]. Typically, haloanilines are known to be basic components and intermediates in organic synthesis [7,8]. Due to their physical properties, their applications extend even to the fields of physics and engineering [4,5,9]. It has been shown by one of us (GJR) that the *N*-protonated form of an halogenaniline and aminopyridines are excellent tectons to stabilize polyhalogenides in the solid state [10]. Thus, halogenated anilines are a versatile class of organic compounds with broad applications in academic research and industry, driving advancements in chemistry, materials science, and pharmaceuticals.

For the field of crystallography, it should be noted, that haloanilines are also frequently used as a component for the design of multicomponent-crystals. The fact that these compounds are able to form co-crystals have been already reported in the 1940ies [11]. A survey in the Cambridge Structural Database [12] showed that especially with haloanilines many multicomponent-crystals are listed [13].

The crystal structures of many pure halogen-substituted anilines have been determined so far. The *ortho*- and *para*- halogen substituted anilines (halogen= Cl, Br, I) were recently investigated [8] in detail. The crystal structures of two *meta*-substituted haloanilines -that are liquid at room temperature- have not yet been described [14]. The class of halogen substituted anilines are still in the focus of interest because of the structure-driving influence of weak interactions [8,14]. It is expected that this class of solids will exhibit hydrogen bonds, halogen bonds, and weaker intermolecular interactions, such as π–π stacking with various strengths. Unlike traditional hydrogen bonds, halogen bonds arise from the electrostatic interaction between the electrophilic region of the halogen atom and the nucleophilic region of the electron donor. This interaction is directional, non-covalent, and characterized by its strength and specificity. Understanding the factors that influence strength and geometry – in generally the energetic approach – allows us to design molecules with tailored binding and packing properties.

This work continues our systematic combination of crystallographic and quantum chemical studies on amino group-containing compounds [15–17] and halogenated anilines [8].

* Corresponding author.
E-mail address: ikonovalova0210@gmail.com (I.S. Konovalova).

https://doi.org/10.1016/j.molstruc.2025.143745
Received 27 June 2025; Received in revised form 20 August 2025; Accepted 21 August 2025
Available online 23 August 2025

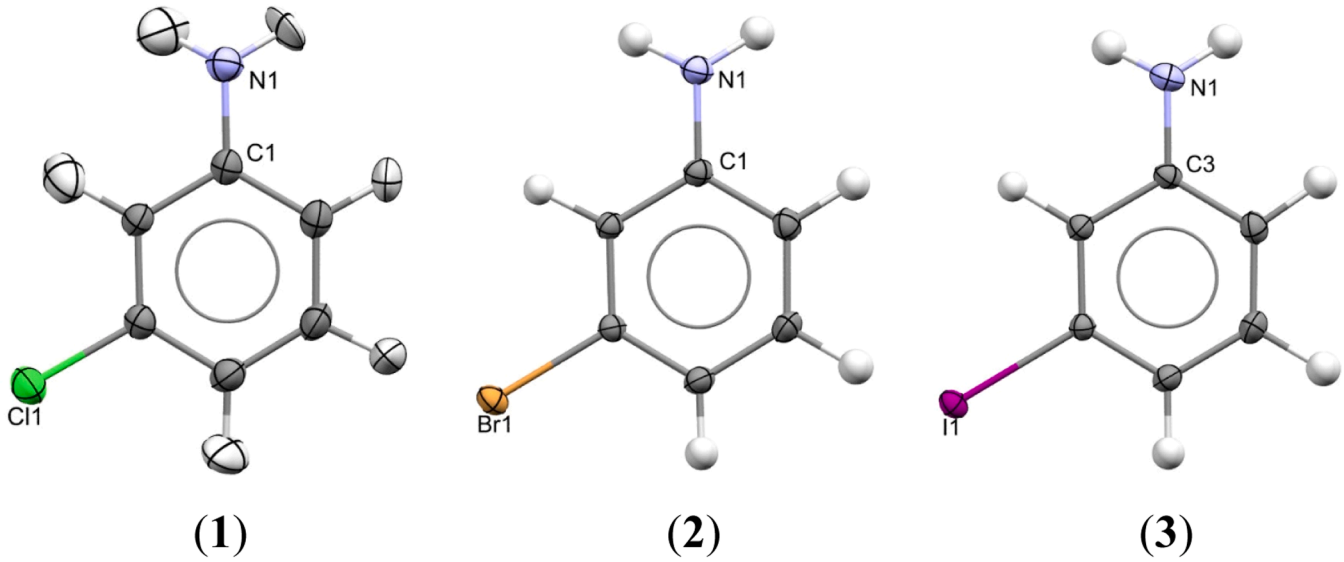

Fig. 1. Molecular structure of compounds **1**-**3**. Thermal ellipsoids are shown at the 50 % probability level.

Table 1
Selected crystallographic data on the studied crystals of compounds **1**-**3.**

N№	Space group	*a*, Å	*b*, Å	*c*, Å	V, Å3	R_1-factor, %
1	*Pbca*	5.0135 (4)	14.5517 (14)	16.5970 (15)	1210.8	3.86
2	$P2_12_12_1$	4.9125 (2)	12.6470 (6)	19.9431 (10)	1239.0	3.06
3	$P2_12_12_1$	5.0652 (4)	12.9018 (9)	20.5219 (15)	1341.1	2.85

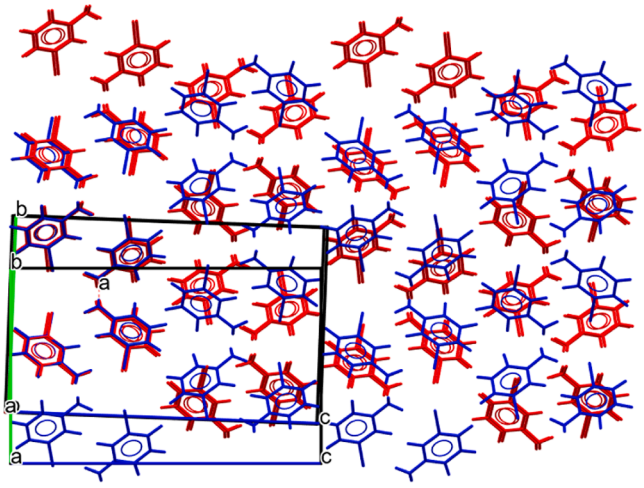

Fig. 2. Superposition of the two structures (blue **3** and red OHEKIZ) viewed along the crystallographic *a*-axis.

2. Experimental section

2.1. Synthesis and crystallization

Compounds where purchased from **1** (3-chloroaniline) TCI Deutschland GmbH (> 99.0 %), **2** (3-bromoaniline) Apollo Scientific Ltd. (98 %), **3** (3-iodoaniline) BLD Pharmatech GmbH (98 %) and used as received. All compounds **1**-**3** (Fig. 1) are liquid at room temperature and atmospheric pressure and are therefore not directly accessible for analysis by means of SC-XRD (single crystal X-ray diffraction). In recent years, we have shown that capillary crystallization is an excellent way of converting liquid compounds into high quality single crystals [18–21]. Differential Scanning Calorimetry (DSC) was used to study the phase behavior of the compounds at low temperatures prior to crystallization.

After initial DSC studies and the measurement of an ATR-FT-IR spectra (see Supporting Information) ca. 10 μL of the liquid was transferred into a borosilicate glass capillary with a diameter of 0.5 mm (WJM-Glas Müller GmbH, Berlin, Germany) mounted on a magnetic base (Hampton Research, Aliso Viejo, CA, USA). The base containing the capillary was then placed on the goniometer head of a four-circle single-crystal X-ray diffractometer. A stream of nitrogen gas from an Oxford Instruments cryostat maintained the capillary at a temperature of 100 K. At this temperature, the capillaries were briefly removed from the cold gas stream and re-inserted several times. This initially coarse cracks in the transparent sample. The samples were then heated above their respective solidification points. This revealed areas, where the glass had transformed into a polycrystalline and dusty powder. The polycrystalline powder was then partially melted by moving the capillary in and out of the cold gas stream, while retaining some solid in the capillary, until the cylinder was filled with a single crystal. The capillary was then rapidly cooled down to 100 K for the collection of the diffraction data. For data acquisition, a fixed chi angle of 54.7° was chosen to ensure that the exposed crystalline volume was as small as possible consistent with a high redundancy.

2.2. Quantum chemical calculations

The analysis of the studied structures was performed using the approach based on calculations of pairwise interaction energies between molecules in a crystal [22–23]. The first coordination sphere for each molecule found in the unit cell asymmetric part (M_0) was determined separately using the standard procedure within the Mercury program (version 4.2) [24] as had been suggested before [22]. The obtained cluster was divided into dimers where one molecule is M_0 and every other molecule M_i belongs to the first coordination sphere. The atomic coordinates of M_0-M_i dimers were taken from the crystal structure.

The interaction energies between molecules within each of M_0-M_i dimers were calculated using B97-D3/Def2-TZVP density functional method [25–29] and corrected for basis set superposition error by the counterpoise method [30]. The B97-D3 functional was benchmarked to be one of the best performing dispersion-corrected density functional for the calculations of various intermolecular interactions [31]. All the

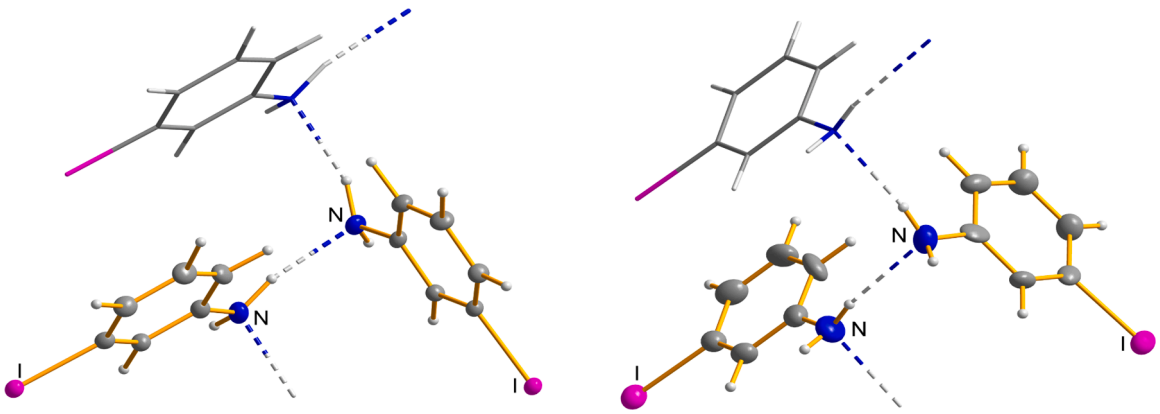

Fig. 3. The two structural models (left: **3**; right: OHEKIZ) in comparison showing the hydrogen bonded *C*(6) chains.

Table 2
Geometrical characteristics of the conjugation degree between amino group and aromatic π-system in compounds **1-3**.

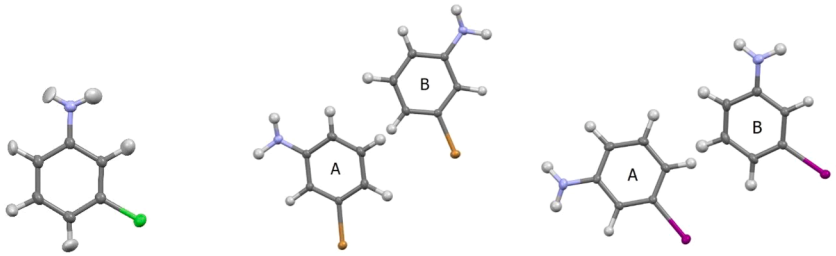

1 **2** **3**

Compound	$d_{C-N1/N3}$, Å	$Angle_{\sum N(1)}$, deg.
1	1.393(2)	345.3
2A	1.394(2)	346.4
2B	1.386(2)	343.5
3A	1.385(3)	339.2
3B	1.382(3)	346.2

calculations were performed with the ORCA 5.0 software [32].

The analysis of the pairwise interaction energies is based on the assumption that the calculated values take on vector properties, [22] because each calculated interaction energy originates from the geometric center of the basic molecule M_0 and is directed to one of the neighboring molecules M_i. All energy vector lengths within the first coordination sphere of the basic molecule are normalized to the strongest pairwise interaction energy using the equation:

$$L_i = (R_i E_i)/2E_{str}$$

where R_i is the distance between the geometrical centers of interacting molecules M_0-M_i, E_i is the interaction energy between two molecules in these pairs and E_{str} is the energy of the strongest pairwise interaction in the crystal structure.

Such a normalization results in the independence of the vector lengths from the calculation method. Application of this approach makes it possible to replace the basic molecule by its vector image and to construct the so-called *energy-vector diagram* [22] of a crystal structure using symmetry operations.

3. Results and discussion

All *meta*-isomers are liquids at room temperature. During thermal analysis (DSC) compounds **1-3** showed a similar behavior. No direct phase transition from liquid to solid was observed during cooling from 25°C to −160°C. Phase transitions could only be observed as exothermic signals during heating and after passing through a glass transition (compound **1** T_g = −89°C, T_s = −56°C; compound **2** T_g = −82°C, T_s= −49°C; compound **3** T_g = −72°C, T_s = −37°C). After a hysteresis of about 60°C, the melting of the crystalline phases could then be observed during further heating (compound **1** T_m = −16°C, compound **2** T_m = 10°C, compound **3** T_m = 17°C). For further details on thermal analysis and thermograms see Supporting Information

Crystals of **1-3** suitable for single-crystal-structure analysis were obtained from the melt at low temperature as described above. The 3-chloroaniline (**1**) crystallizes in the centrosymmetric space group *Pbca* and the 3-bromo-, 3-iodoaniline (**2, 3**) crystallizes in the non-centrosymmetric space group $P2_12_12_1$ (Table 1). In crystal **1** there is only one molecule in the independent part of the unit cell. The crystal structures of compounds **2-3** consist of two independent molecules per unit cell (A and B) (Fig. 1) and are isostructural.

3.1. Explanation for the redetermination of the structure of meta-iodoaniline (3-Iodoaniline) 3

When our experiments were already completed, the structure of 3-iodoaniline (**3**) at 200 K was reported [33] with Ref. code OHEKIZ (CCDC No. 2411477). The authors describe the structure in space group $P2_12_12_1$ (No. 19), which has a unit cell with the following dimensions: a = 5.0748(3) Å, b = 12.9872(8) Å and c = 20.6243(12) Å, with Z = 8 per unit cell. This was reproduced in our investigation within the standard errors. Superposition of the two structures using the Structure Overlay

Table 3
Intermolecular interactions and their geometric characteristics in the crystals of compounds **1**-**3**.

Compound	Interaction	Symmetry operation	$d_{H\cdots A}$, Å	angle $_{D\text{-}H\cdots A}$, deg.
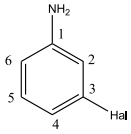				
1	N1-H1NA ···$N1_{LP}$	0.5+*x*,*y*,0.5-*z*	2.17	163
	N1-H1NA···Cl1	1.5-*x*,0.5+*y*,*z*	2.74	143
	N1-H1NB···Cl1	0.5-*x*,0.5+*y*,*z*	2.98	112
	C2-H2···C2(π)	0.5+*x*, *y*,0.5-*z*	2.57	175
	C2-H2···C1(π)	0.5+*x*, *y*,0.5-*z*	2.66	151
	C5-H5···C6(π)	0.5+*x*,0.5-*y*,1-*z*	2.74	140
2	N1A-H1AA···$N1B_{LP}$	0.5+*x*,1.5-*y*,1-*z*	2.10	166
	C5A-H5A···C5A (π)	0.5+*x*,1.5-*y*,1-*z*	2.72	132
	C4A-H4A···C5B (π)	0.5+*x*,1.5-*y*,1-*z*	2.77	126
	N1A-H1AB···C2B (π)	0.5-*x*,1-*y*,0.5+*z*	2.73	132
	N1B-H1BB···$N1A_{LP}$	0.5+*x*,1.5-*y*,1-*z*	2.08	166
	N1B-H1BA···C2A (π)	0.5-*x*,1-*y*,-0.5+*z*	2.80	126
	C4B-H4B···Br1B	-0.5+*x*,0.5-*y*,1-*z*	3.14	130
	Br1B···C5B(π)	-1+*x*,*y*,*z*	3.64	
	Br1A···Br1B	-0.5+*x*,0.5-*y*,1-*z*	3.57	169
	Br1A···Br1B	-0.5+*x*,0.5-*y*,1-*z*	3.71	172
3	N1A-H1AA···$N1B_{LP}$	0.5+*x*,1.5-*y*,1-*z*	2.16	160
	C5A-H5A···C5A (π)	-0.5+*x*,1.5-*y*,1-*z*	2.67	136
	C5A-H5A···C4A (π)	-0.5+*x*,1.5-*y*,1-*z*	2.75	134
	C4A-H4A···C5B (π)	*x*,*y*,*z*	2.77	125
	N1A-H1AB···C2B (π)	1.5-*x*,1-*y*,-0.5+*z*	2.86	138
	N1B-H1BB···$N1A_{LP}$	0.5+*x*,1.5-*y*,1-*z*	2.16	164
	N1B-H1BA···C2A (π)	1.5-*x*,1-*y*,-0.5+*z*	2.94	131
	C4B-H4B···I1B	-0.5+*x*,0.5-*y*,1-*z*	3.19	140
	N1B-H1BA···I1A	1-*x*,0.5+*y*,0.5-*z*	3.21	142
	I1B···C5B(π)	0.5+*x*,1.5-*y*,1-*z*	3.76	
	I1A···I1B	-0.5+*x*,0.5-*y*,1-*z*	3.76	172
	I1A···I1B	-0.5+*x*,0.5-*y*,1-*z*	3.83	173

tool in Mercury 2023.2.0 [24] produced a good overall match (Fig. 2; RMS = 0.017). Due to the different measurement temperatures, slight differences are expected.

However, closer examination of the published structure revealed that it would be beneficial to rely on our own newly collected and interpreted data for this comparative investigation, as the structure reported in the literature appears to have some minor issues. Initially, our dataset on 3-iodoaniline **3** was of sufficient quality to be refined using the non-spherical atomic form factors implemented in the NoSpherA2 module of OLEX2 [34–36]. Using this non-spherical atomic form factor approach in our refinement process provides significantly better model, as reflected by the much smaller errors in bond lengths and angles and even in some absolute geometric parameters. The structure exhibit a hydrogen-bonding chain motif that can be classified as C(4) according to Etter's graph-set nomenclature (Fig. 3). Surprisingly, in the previously reported structure, the longest N–H bond distance (d_{N1H1B} = 0.92(13) Å) in the -NH_2 groups is found for a hydrogen atom that is not involved in one of the hydrogen bonds forming the aforementioned chain. In contrast, our newly determined structural model shows that the N–H bond distances of hydrogen atoms involved in hydrogen bonding are slightly longer (d_{N1H1a} = 1.02(5) Å and d_{N2H2b} = 1.01(5) Å) than those engaged only in weak interactions (d_{N1H1b} = 0.99(4) Å and d_{N2H2a} = 0.97(4) Å), which is in agreement with our expectations. Furthermore, some ellipsoids (e.g. C11 and C21, bonded to the NH_2 group) show the largest amplitudes of the displacement tensors along the bonding directions of the neighbouring bonded atoms in the published structure appear to be affected by crystallographic issues. The data quality in our report has improved as we have refined 181 parameters against 8.391 unique reflections, compared to the 157 parameters that were refined against 3.379 reflections in the previously reported structure [33]. Another issue is that five reflections were omitted from the reported dataset prior to the final refinement. The reported structure was ultimately refined as an inversion twin with a BASF value of 0.44(9). This could potentially be due to low Friedel pair coverage and insignificant intensity differences, or incorrect merging during data processing. The herein reported data set has a high Friedel pair coverage and results in an acceptable absolute structure parameter of Flack *x* = -0.021(8).

3.2. Molecular structure analysis

The ability of the amino group to participate in intermolecular interactions as a proton donor and/or acceptor is significantly driven by the extent of n-π conjugation between the nitrogen lone pair and the aromatic π-system. It is well known that this conjugation is affected by the surrounding polarizing environment [16,37,38]. Key indicators of conjugation strength include the C–N bond length and the geometrical

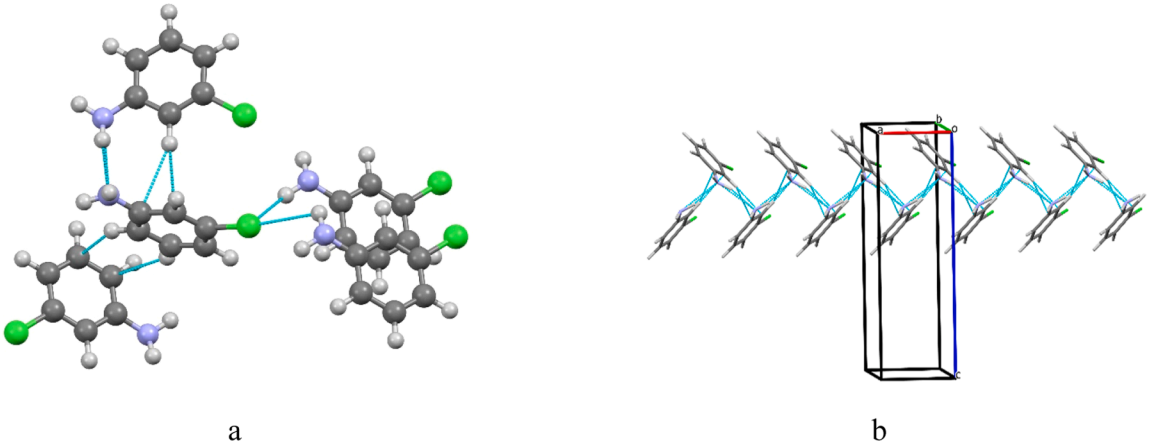

a b

Fig. 4. Packing of molecules **1** in the crystalline phase: a) short contacts (blue lines); b) zig-zag chains, view along the *b* crystallographic direction. Color code: green: chlorine, blue: nitrogen, gray: carbon, white: hydrogen.

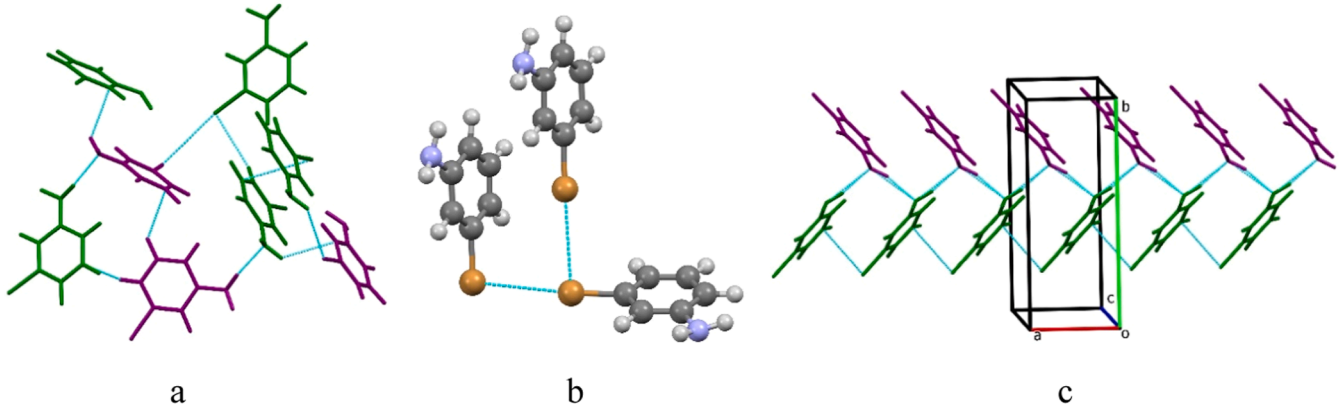

Fig. 5. Packing of molecules **2** in the crystalline phase: a) short contacts; b) bifurcated halogen bond; c) zig-zag chains, view along the *c* crystallographic direction. Violet: molecule A, green: molecule B. Color code: brown: bromine, blue: nitrogen, gray: carbon, white: hydrogen.

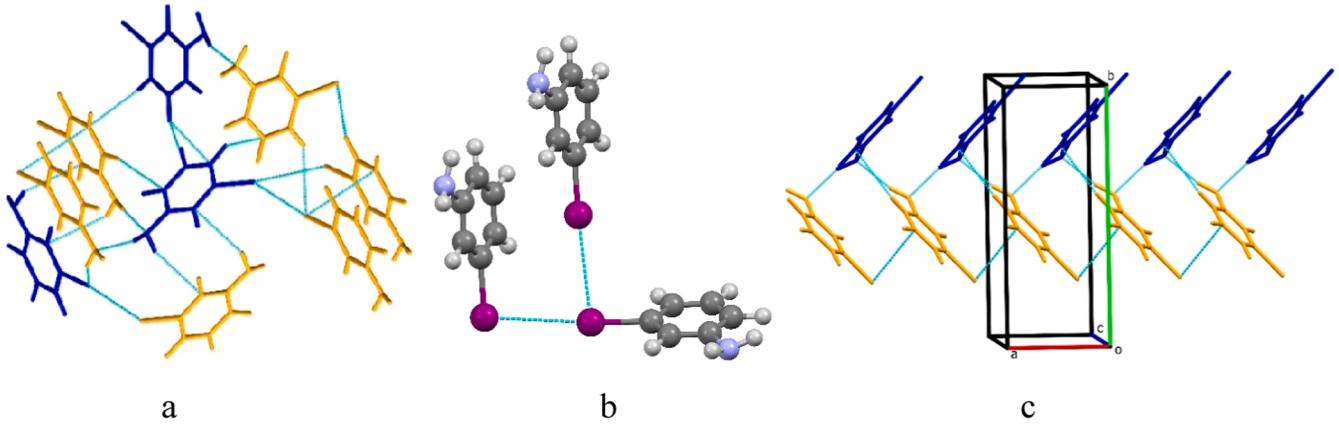

Fig. 6. Packing of molecules 3 in the crystalline phase: a) short contacts; b) bifurcated halogen bond; c) a zigzag chain view along the *c* crystallographic direction. Blue: molecule A, yellow: molecule B. Color code: purple: iodine, blue: nitrogen, gray: carbon, white: hydrogen.

Table 4
Symmetry codes, interaction type, interaction energy of the basic building unit with neighbouring ones (E_{int}, kcal/mol) with the highest values (more than 5 % of the total interaction energy) and the contribution of this energy to the total interaction energy (%) in the crystal of **1** (*ER*).

Dimer	Symmetry operation	Interaction Energy E(int), kcal/mol	ER, %	Interaction
1-d1	-1/2+x,y,1/2-z	-5.44	13.0	N1-H…N1 2.17 Å, 163°, C-H…π 2.62 Å, 175°
1-d2	1/2+x,y,1/2-z	-5.44	13.0	N1-H…N1 2.17 Å, 163°, C-H…π 2.62 Å, 175°
1-d3	-1/2+x,1/2-y,1-z	-3.51	8.4	C4-H…C3(π) 2.74 Å, 140°
1-d4	1/2+x,1/2-y,1-z	-3.51	8.4	C4-H…C3(π) 2.74 Å, 140°
1-d5	1+x,y,z	-3.35	8.0	non-specific
1-d6	-1+x,y,z	-3.35	8.0	non-specific
1-d7	3/2-x,-1/2+y,z	-2.95	7.1	N1-H…Cl 2.71 Å, 143°
1-d8	3/2-x,1/2+y,z	-2.95	7.1	N1-H…Cl 2.71 Å, 143°
1-d9	1-x,1-y,1-z	-2.74	6.6	non-specific

configuration of the nitrogen atom: planar or pyramidal. When conjugation is strong, the C–N bond becomes shorter than expected based on formal valence considerations. In such cases, the nitrogen atom adopts a planar configuration, aligning itself with the ring carbon atom and the two hydrogen atoms to which it is attached. The analysis of the molecular structures **1**-**3** revealed that the C–NH_2 bond lengths range from 1.382(3) to 1.394(2) Å, while the sum of bond angles around the nitrogen atom varies between 339.2° and 346.4° (Table 2). Such variation suggests that the conjugation between the amino group and the aromatic ring is relatively weak. This conclusion is further supported by the C_{ar}–N bond lengths (Table 2) and the pyramidal conformation of the nitrogen atoms. Consequently, the amino group is expected to participate in hydrogen bonding as a proton donor as well as acceptor in all examined structures. Similar amino group parameters have been reported in previous studies on certain amino-pyridines, *para*-chloro, *ortho*-bromo- and *ortho*-iodoaniline [8].

It is important to note that the geometrical characteristics of amino groups, such as the X–NH_2 bond length, are also influenced by the formation of intermolecular interactions. Therefore, a quantitative analysis of these interactions has been conducted.

3.3. Crystal structure analysis of compounds 1–3 based on studying of geometrical characteristics of intermolecular interactions

The presence of a halogen atom in the *meta*-position of an aniline suggests the potential formation of halogen bonds (X-bonds [39]) and hydrogen bonds (H-bonds), where the halogen substituent acts as a proton acceptor.

Analysis of intermolecular interactions revealed that in the 3-chloroaniline crystal (**1**), only N–H···Cl hydrogen bonds were observed (Table 3). In contrast, the crystals of compounds **2** and **3** exhibited a

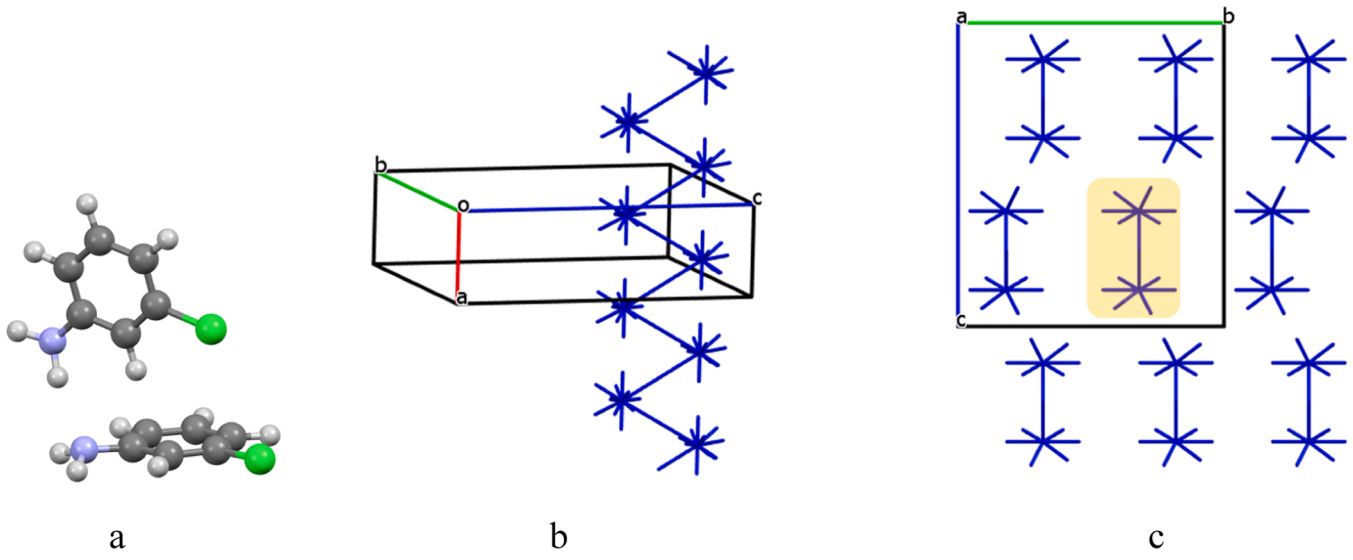

Fig. 7. The 1-d1dimer with the strongest interaction in structure **1** (*a*), zig-zag column (*b*), packing in terms of energy-vector diagrams, projection along the *a* crystallographic direction (*c*). The double column is highlighted in yellow.

Table 5
Symmetry codes, interaction type, interaction energy of the basic building unit with neighbouring ones (E_{int}, kcal/mol) with the highest values (more than 5 % of the total interaction energy) and the contribution of this energy to the total interaction energy (%) in the crystal of **2** (*ER*).

Dimer	Symmetry operation	Interaction Energy E(int), kcal/mol	ER, %	Interaction
Monomeric building unit (MBU)				
2-d1	1/2-x,1-y,1/2+z	-8.02	8.9	N-H…π 2.72 Å, 132°; N-H…π 2.80 Å, 126°
2-d2	1/2-x,1-y,-1/2+z	-8.02	8.9	N-H…π 2.72 Å, 132°; N-H…π 2.80 Å, 126°
2-d3	3/2-x,1-y,-1/2+z	-4.72	5.2	N1-H…Br 2.99 Å, 142°; N1-H…Br 3.12 Å, 136°
2-d4	3/2-x,1-y,1/2+z	-4.72	5.2	N1-H…Br 2.99 Å, 142°; N1-H…Br 3.12 Å, 136°
2-d5	-1/2+x,3/2-y,1-z	-4.61	5.1	N1-H…N1 2.07 Å, 166°
2-d6	1/2+x,3/2-y,1-z	-4.61	5.1	N1-H…N1 2.07 Å, 166°
2-d7	1/2+x,3/2-y,1-z	-4.52	5.0	N1-H…N1 2.09 Å, 166°
2-d8	-1/2+x,3/2-y,1-z	-4.52	5.0	N1-H…N1 2.09 Å, 166°
Dimeric building unit (DBU)				
2-dd1	1+x,y,z	-12.94	17.2	N1-H…Br 2.99 Å, 142°, non-specific
2-dd2	-1+x,y,z	-12.94	17.2	N1-H…Br 2.99 Å, 142°, non-specific
2-dd3	1-x,-1/2+y,1/2-z	-7.58	10.1	N1-H…N1 2.09 Å, 166°, Br…Br 3.71Å
2-dd4	1-x,1/2+y,1/2-z	-7.58	10.1	N1-H…N1 2.09 Å, 166°, Br…Br 3.71Å
2-dd5	-x,1/2+y,1/2-z	-7.34	9.8	N1-H…N1 2.07 Å, 166°, Br…Br 3.57Å
2-dd6	-x,-1/2+y,1/2-z	-7.34	9.8	N1-H…N1 2.07 Å, 166°, Br…Br 3.57Å

broader range of interactions, including C/N–H···Hal hydrogen bonds, Hal···π interactions, and halogen···halogen (Hal···Hal) contacts - commonly referred to as halogen bonds (XBs) - with comparable geometric parameters (Table 3). Among these, the I···I halogen bond observed in compound **3** was found to be the strongest, based on its geometric features (Table 3). Recent studies have highlighted the important role of Hal···π and C–H···π interactions in shaping the supramolecular architecture of crystals, underscoring the need for detailed investigation of these weak interactions [40,41].

As anticipated from amino group's geometrical characteristics, N–H···NH_2 hydrogen bonds were present in all crystal structures (Table 3). The strongest of these bonds was observed in the crystal of compound **2**, due to its geometric parameters.

Based on the geometrical characteristics, the molecules in compound **1** primarily form weak intermolecular interactions. The only relatively strong interaction observed is the N1–H1NA···$N1_{LP}$ hydrogen bond, in which the amino group simultaneously acts as both an bifunctional proton donor and an acceptor (Table 3, Fig. 4a). As a result, due to the C2-H2···π and N1-H1NA···$N1_{LP}$ hydrogen bonds zig-zag chains along *a* crystallographic direction are recognized as a main packing motif in the crystal structure of **1** (Fig. 4b).

The presence of bromine and iodine atoms in the *meta*-position of molecules **2** and **3**, along with the presence of two independent molecules in the asymmetric unit, leads to an increase in the number of intermolecular interactions (Table 3). The types and geometric characteristics of these interactions are quite similar across both structures (Fig. 5a and 6a).

By comparing the strength of these interactions using average *van der Waals* radii for halogen atoms based on various approaches [42], we can conclude that the halogen interactions in these structures are relatively strong. Furthermore, when comparing *meta*-substituted haloanilines with recently published *ortho*- and *para*-substituted analogs, it is evident that the geometrical characteristics of halogen bonds remain similar [8]. However, in the crystals of compounds **2** and **3**, we observed the presence of bifurcated halogen bonds (Table 3, Fig. 5b, 6b). Such type of interactions was found in analogues molecules [43,44].

The analysis of intermolecular interactions in crystals **2** and **3** revealed that the amino group simultaneously acts as an amphoteric proton donor and acceptor, with all hydrogen atoms fully engaged in hydrogen bonding. The σ-hole of halogen atoms participate not only in Hal···Hal halogen bonds but also in Hal···π interactions and non-classical C/N–H···Hal hydrogen bonds. Additionally, weak C/N–H···π hydrogen bonds were identified (Table 3). Given that the N–H···N_{LP} hydrogen bonds are the strongest in these crystals, zig-zag columns along the *a* crystallographic direction can be distinguished (Fig. 5c, 6c). Within these columns, the molecules are connected by N1–H1N···N_{LP}, C–H···π, and Hal···π interactions. A visual analysis suggests that the packing of crystals **2** and **3** appear to be isostructural.

Notably, stacking interactions are absent in the structures of *meta*-substituted haloanilines, despite the presence of an aromatic π-system

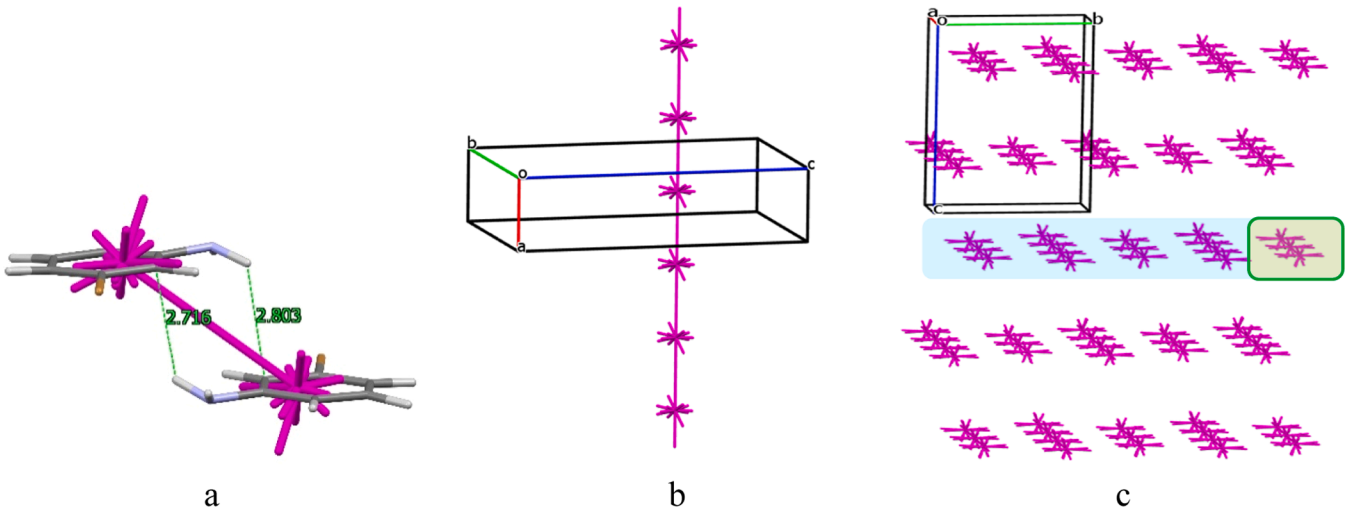

Fig. 8. The 2-d1 dimer as the building unit in structure **2** (a), a column as the first basic structural motif (b), the layers of dimers shown as energy-vector diagrams (*c*). The layers are highlighted blue and columns are highlighted in yellow.

Table 6
Symmetry codes, interaction type, interaction energy of the basic building unit with neighbouring ones (E_{int}, kcal/mol) with the highest values (more than 5 % of the total interaction energy) and the contribution of this energy to the total interaction energy (%) in the crystal of **3** (*ER*).

Dimer	Symmetry operation	Interaction Energy E (int), kcal/mol	ER, %	Interaction
Monomeric building unit (MBU)				
3-d1	3/2-x,1-y,1/2+z	-8.22	8.4	N-H…π 2.83 Å, 138°; N-H…π 2.91 Å, 130°
3-d2	3/2-x,1-y,-1/2+z	-8.22	8.4	N-H…π 2.83 Å, 138°; N-H…π 2.91 Å, 130°
3-d3	1/2-x,1-y,1/2+z	-5.30	5.4	N-H…I 3.18 Å, 142°; N-H…I 3.27 Å, 135°
3-d4	1/2-x,1-y,-1/2+z	-5.30	5.4	N-H…I 3.18 Å, 142°; N-H…I 3.27 Å, 135°
3-d5	1/2+x,3/2-y,1-z	-5.07	5.2	N-H…N 2.16 Å, 164°
3-d6	-1/2+x,3/2-y,1-z	-5.07	5.2	N-H…N 2.16 Å, 164°
Dimeric building unit (DBU)				
3-dd1	-1+x,y,z	-14.43	17.5	N-H…I 3.18 Å, 142°, non-specific
3-dd2	1+x,y,z	-14.43	17.5	N-H…I 3.18 Å, 142°, non-specific
3-dd3	1-x,1/2+y,1/2-z	-8.50	10.3	N-H…N 2.16 Å, 164°, I…I 3.76Å
3-dd4	1-x,-1/2+y,1/2-z	-8.50	10.3	N-H…N 2.16 Å, 164°, I…I 3.76Å
3-dd5	2-x,1/2+y,1/2-z	-8.40	10.2	N-H…N 2.09 Å, 166°, I…I 3.71Å
3-dd6	2-x,-1/2+y,1/2-z	-8.40	10.2	N-H…N 2.09 Å, 166°, I…I 3.71Å

(Table 3). A similar lack of stacking interactions has been observed in *para*-haloanilines [8], all isomers of diaminobenzenes, and mono-aminopyridines [15–17].

Key conclusions from a geometric perspective of the crystal structure study:

a) Stacking interactions are absent in all *meta*-substituted haloanilines;
b) The amino group consistently acts as both a proton donor and a proton acceptor in hydrogen bonding.
c) Halogen bonds were not observed in the crystal of compound **1**, whereas strong bifurcated halogen bonds were present in the crystals of compounds **2** and **3**.
d) Geometric analysis alone is insufficient to draw definitive conclusions about main structural motifs in crystal packing and tends to underestimate the role of weak interactions. The diversity of these interactions complicates direct comparisons and makes it difficult to identify the most significant one.

3.3. Crystal structure analysis of compounds 1–3 based on an energetic viewpoint

As mentioned earlier, analyzing geometric characteristics is not always the most effective approach for studying the peculiarities of crystal packing when multiple weak interactions are present. A more efficient method is the analysis of interaction energies between neighboring molecules, calculated using *ab initio* methods [15–17,22,23]. The key advantage of this approach is its independence from the specific nature of the interactions, while accounting for all existing interactions (such as hydrogen bonding, dispersion, electrostatic interactions, polarization, etc.). Additionally, this method can be applied not only to individual molecules as simple building units (BU) of a crystal packing but also to more complex BUs like dimers, trimers, or tetramers of molecules [22].

The first coordination sphere for each of the building units (molecule or dimer) which is located in the asymmetric part of the unit cell across all studied crystals contains 14 neighboring units. Selected data for the dimers, where the interaction energies are stronger than 5 % of the total interaction energy of the basic molecule with all molecules in its first coordination sphere, are presented in Tables 4-6.

The total interaction energy of molecule **1** with its 14 neighboring molecules is -41.7 kcal/mol. Pairwise interaction analysis shows that two strongest interactions (N-H···N, C-H···π) occur with molecules positioned in opposite directions (Table 4, Fig. 7a). Each of these interactions has an energy of -5.44 kcal/mol, forming a double zig-zag column, which serves as the primary structural motif (BSM) in the crystal of **1** (Fig. 7b). The bond angle between the central molecule and its strongly bound neighbors is 60.3°, closely matching the structure of *para*-iodoaniline reported recently [40]. Within the double column, the total interaction energy is -17.6 kcal/mol. The interaction energy between neighboring columns is weaker (-4.6 to -7.0 kcal/mol) and mainly stabilized by N–H···Cl and C–H···π hydrogen bonds (Fig. 7b). Additionally, Cl···N and non-specific interactions further contribute to the overall stability of the columns. Thus, the crystal of **1** can be classified as columnar, with only one level of structural organization (Fig. 7c).

In structure **2**, the total interaction energy of two independent basic molecules, A and B, with the 28 molecules in first coordination sphere is -90.0 kcal/mol. Analyzing the pairwise interaction energies between the

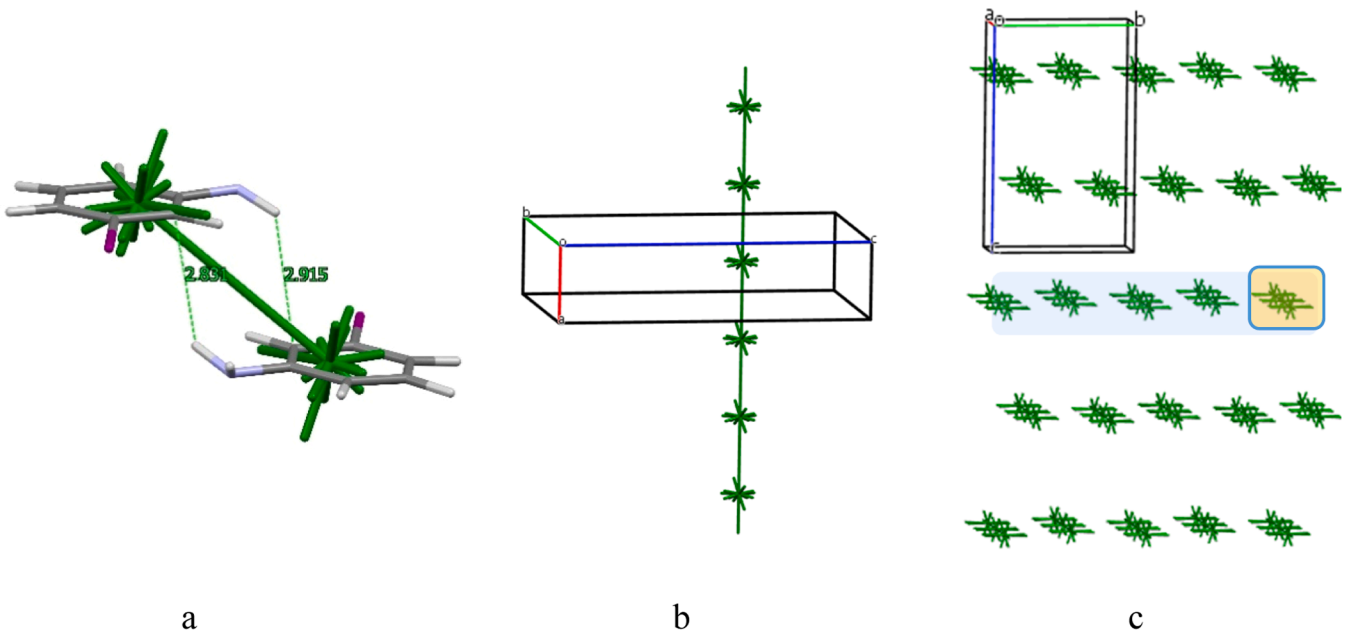

Fig. 9. The 3-d1 dimer with the strongest interaction in structure **3** (a), The 3-d3 dimer (b), zig-zag column (b), packing in terms of energy-vector diagrams, projection along the *b* crystallographic direction. The double columns are highlighted in green.

basic molecule and its neighboring molecules revealed that the strongest interaction occurs in dimer 2_d1 (Table 5). This dimer has an interaction energy of -8.2 kcal/mol, which is nearly twice as strong as the interaction energy between the basic molecule and any other neighbor. Due to the N-H···π hydrogen bonds, this centrosymmetric dimer can be considered as a dimeric building unit of structure **2** (Fig. 8a).

The next step in the analysis involved constructing the first coordination sphere around this dimer. It is surrounded by 14 neighboring dimers, with a total interaction energy of -75.0 kcal/mol. Among these, the dimer forms the strongest interactions with two others (Table 5), leading to the formation of a linear column of dimers. This column serves as the primary basic structural motif (BSM) in the crystal of structure **2** (Fig. 8b). Within this column, the interaction energy between adjacent dimers is -25.9 kcal/mol. These columns align to form layers parallel to the (0 0 1) crystallographic plane, with an interaction energy of -55.7 kcal/mol (Fig. 8c). Within the layer, dimers are held together by N-H···N and N-H···Br hydrogen bonds, Br···Br halogen bonds, and non-specific interactions. The interactions between neighboring layers are weaker (-19.3 kcal/mol) and involve C-H···π, C-H···Br hydrogen bonds, and non-specific interactions. As a result, the crystal packing of structure **2** exhibits two levels of organization and can be classified as columnar-layered (Fig. 8c).

Similar to structure **2**, the crystals of structure **3** contain two independent molecules, A and B, in the asymmetric unit. The first coordination sphere of the basic dimer includes 28 neighboring molecules. The total interaction energy of the basic molecules A and B with all surrounding molecules is slightly higher than in structure **2** (-98.4 kcal/mol). Both molecules form centrosymmetric N–H···π dimers (3-d1, 3-d2), identical to those observed in structure **2** (Table 6). Consequently, this dimer is also considered the initial dimeric building unit of structure **3** (Fig. 9a).

As in the crystal structure of compound **2**, a column can be identified as the primary basic structural motif in structure **3** (Fig. 9b). However, the interaction energy of the basic molecule within this column is slightly bigger (-28.9 kcal/mol). These columns are interconnected into layers via N–H···N_{LP}, N–H···I hydrogen bonds, and I···I halogen bonds. The interaction energy of the basic molecule within the layer is -62.7 kcal/mol. In contrast, the interaction energy between adjacent layers is three times lower (-19.8 kcal/mol) and is sustained by weaker C–H···π and C–H···I hydrogen bonds, along with various non-specific interactions. Thus, structure **3** can also be classified as columnar-layered (Fig. 9c). It is noteworthy that the crystal packing principles of *meta*-bromo and -iodo anilines are isostructural, exhibiting the same supramolecular architectures and structural motifs.

4. Conclusions

In summary, we have determined the solid-state structures of *meta*-haloanilines (Cl, Br for the first time and re-determination of I). Molecular analysis and crystal structure studies from a geometric perspective reveal that the amino groups participate in hydrogen bonding, acting as amphoteric proton donors and acceptors in all examined structures. Interestingly, no stacking interactions were observed in any of the *meta*-substituted haloanilines. Additionally, strong bifurcated halogen bonds were observed only in the bromine- and iodine-substituted compounds.

Crystal packing analysis from an energetic perspective shows that the type of building unit, basic structural motifs, and overall packing organization differ among crystals **1-3**. In the crystal structure of *meta*-chloroaniline (**1**), double columns were identified as the primary structural motif, with N–H···N and C–H···π hydrogen bonds playing a dominant role in crystal formation. The crystal packings of *meta*-bromoaniline and *meta*-iodoaniline are isostructural, exhibit two levels of organization, and can be classified as columnar-layered. In these structures, N–H···π, N–H···Hal, and N–H···N hydrogen bonds, along with halogen bonds, play a central role in crystal formation. In contrast, weaker C–H···π and C–H···Hal hydrogen bonds, as well as various non-specific interactions, contribute only marginally, mainly by connecting neighboring layers.

Supporting Information

The Supporting Information contains DSC experiments data of compounds **1-3** (page S2-S4), X-ray Crystal Structure Analysis of compounds **1-3** (page S5-S22) and AT-FTIR spectra (page S23-S24).

CRediT authorship contribution statement

Irina S. Konovalova: Writing – original draft, Supervision, Investigation, Conceptualization. **Nils Nöthling:** Writing – review & editing, Visualization, Investigation. **Guido J. Reiss:** Writing – review & editing, Visualization, Validation, Investigation, Data curation.

Declaration of competing interest

The authors declare the following financial interests/personal relationships which may be considered as potential competing interests: Irina S. Konovalova reports financial support and equipment, drugs, or supplies were provided by Heinrich Heine University Düsseldorf. Irina S. Konovalova reports a relationship with Heinrich Heine University Düsseldorf that includes: employment and funding grants. If there are other authors, they declare that they have no known competing financial interests or personal relationships that could have appeared to influence the work reported in this paper.

Acknowledgements

This project has received funding through the MSCA4Ukraine project, which is funded by the European Union. The views and opinions expressed are those of the author(s) only and do not necessarily reflect those of the European Union. Neither the European Union nor the MSCA4Ukraine Consortium as a whole nor any individual member institutions of the MSCA4Ukraine Consortium can be held responsible for them. NN thanks the Max Planck Institut für Kohlenforschung and its board of dircetors for the use of the infrastructure and equipment.

Supplementary materials

Supplementary material associated with this article can be found, in the online version, at doi:10.1016/j.molstruc.2025.143745.

Data availability

Data will be made available on request.

References

[1] K.G. Neoh, E.T. Kang, K.L. Tan, Chemical copolymerization of aniline with halogen-substituted anilines, Eur. Polym. J. 26 (1990) 403–407, https://doi.org/10.1016/0014-3057(90)90041-2.
[2] H. Reed, T.R. Paul, W.S. Chain, Synthesis of halogenated anilines by treatment of N,N-dialkylaniline N-oxides with thionyl halides, J. Org. Chem. 83 (2018) 11359–11368, https://doi.org/10.1021/acs.joc.8b01590.
[3] S. Pusztai, T. Dankházi, G. Farsang, The electrooxidation of halogeno-anilines at microelectrodes in acetonitrile solution, Electroanalysis 15 (2003) 539–543, https://doi.org/10.1002/elan.200390066.
[4] A. Katsuki, Y. Kobori, S. Tero-Kubota, S. Milikisyants, H. Paul, U.E. Steiner, Magnetic field and spin effects from sequential p-type and d-type triplet mechanisms, Mol. Phys. 100 (2002) 1245–1259, https://doi.org/10.1080/00268970110113579.
[5] S. Kaluva, V.L. Karri, M. Naganathappa, Theoretical investigation of NLO and spectroscopic properties of halogenated aniline, Opt. Quant. Electron. 55 (2023) 874, https://doi.org/10.1007/s11082-023-05132-w.
[6] K.J. Rajimon, N. Elangovan, A.A. Khairbek, R. Thomas, Schiff bases from chlorine substituted anilines and salicylaldehyde: synthesis, characterization, fluorescence, thermal features, biological studies and electronic structure investigations, J. Mol. Liq. 370 (2023) 121055, https://doi.org/10.1016/j.molliq.2022.121055.
[7] M.Y. Fang, L.P. Chen, L. Huang, D.M. Fang, X.Z. Chen, B.Q. Wang, C. Feng, S. K. Xiang, Synthesis of tribenzo[b,d,f]azepines via palladium-catalyzed annulation reaction of 2-iodobiphenyls with 2-halogenoanilines, J. Org. Chem. 86 (2021) 9096–9106, https://doi.org/10.1021/acs.joc.1c01082.
[8] I.S. Konovalova, G.J. Reiss, Halogen bonds versus hydrogen bonds in the crystal packing formation of halogen substituted anilines, Z. Kristallogr. – Cryst. Mater. 240 (2025) 87–100, https://doi.org/10.1515/zkri-2024-0119.
[9] S. Ranjan, S. Takamizawa, Two-dimensional organoferroelasticity in a single crystal of 4-iodoaniline, Cryst. Growth Des. 22 (2022) 1831–1836, https://doi.org/10.1021/acs.cgd.1c01394.
[10] G.J. Reiss, Halogen and hydrogen bonding in the layered crystal structure of 2-iodoanilinium triiodide, $C_6H_7I_4N$, Z. Kristallogr. – N. Cryst. Struct. 234 (2019) 899–902, https://doi.org/10.1515/ncrs-2019-0127.
[11] H.M. Powell, G. Huse, P.W. Cooke, The crystal structure of p-iodoaniline–s-trinitrobenzene, J. Chem. Soc. (1943) 153–157, https://doi.org/10.1039/JR9430000153.
[12] C.R. Groom, I.J. Bruno, M.P. Lightfoot, S.C. Ward, The Cambridge Structural Database, Acta Crystallogr. B72 (2016) 171–179, https://doi.org/10.1107/S2052520616003954.
[13] A.R. Choudhury, D.S. Yufit, J.A.K. Howard, In situ co-crystallization of cresols with aniline and fluoroanilines: subtle interplay of strong and weak hydrogen bonds, Z. Kristallogr. – Cryst. Mater. 229 (2014) 625, https://doi.org/10.1515/zkri-2014-1721.
[14] S.K. Nayak, S.J. Prathapa, T.N.G. Row, In situ cryocrystallization of low melting chloro- and bromo-substituted anilines, J. Mol. Struct. 935 (2009) 156–161, https://doi.org/10.1016/j.molstruc.2009.07.008.
[15] S.V. Shishkina, I.S. Konovalova, O.V. Shishkin, A.N. Boyko, Acceptor properties of amino groups in aminobenzene crystals: study from the energetic viewpoint, CrystEngComm 19 (2017) 6274–6282, https://doi.org/10.1039/C7CE01382E.
[16] S.V. Shishkina, I.S. Konovalova, O.V. Shishkin, A.N. Boyko, Influence of substituents on the acceptor properties of the amino groups in the diaminobenzene analogues, CrystEngComm 19 (2017) 7162–7171, https://doi.org/10.1039/C7CE01732D.
[17] I.S. Konovalova, E.N. Muzyka, V.V. Urzhumtseva, S.V. Shishkina, Role of intermolecular interactions in formation of mono- and diaminopyridine crystals: study from the energetic viewpoint, Struct. Chem. 32 (2021) 235–244, https://doi.org/10.1007/s11224-020-01625-6.
[18] R.W. Seidel, R. Goddard, N. Nöthling, C.W. Lehmann, In situ cryocrystallization and solid-state structures of furfural and some derivatives, CrystEngComm 21 (2019) 3295–3303, https://doi.org/10.1039/C9CE00435A.
[19] Y. Kraemer, C. Ghiazza, A.N. Ragan, S. Ni, S. Lutz, E.K. Neumann, J.C. Fettinger, N. Nöthling, R. Goddard, J. Cornella, C.R. Pitts, Strain-release pentafluorosulfanylation and tetrafluoro(aryl)sulfanylation of [1.1.1]propellane: reactivity and structural insight, Angew. Chem. Int. Ed. 61 (2022) e202211892, https://doi.org/10.26434/chemrxiv-2022-2qmq3.
[20] T. Zheng, N. Nöthling, Z. Wang, B. Mitschke, M. Leutzsch, B. List, A solid noncovalent organic double-helix framework catalyzes asymmetric [6 + 4] cycloaddition, Science 385 (2024) 765–770, https://doi.org/10.1126/science.adp1127.
[21] N. Luo, M. Turberg, M. Leutzsch, B. Mitschke, S. Brunen, V.N. Wakchaure, N. Nöthling, M. Schelwies, R. Pelzer, B. List, The catalytic asymmetric polyene cyclization of homofarnesol to ambrox, Nature 632 (2024) 795–801, https://doi.org/10.1038/s41586-024-07757-7.
[22] O.V. Shishkin, R.I. Zubatyuk, S.V. Shishkina, V.V. Dyakonenko, V.V. Medviediev, Role of supramolecular synthons in the formation of the supramolecular architecture of molecular crystals revisited from an energetic viewpoint, Phys. Chem. Chem. Phys. 16 (2014) 6773, https://doi.org/10.1039/C3CP55390F.
[23] I.S. Konovalova, S.V. Shishkina, M. Wyshusek, M. Patzer, G.J. Reiss, Supramolecular architecture of theophylline polymorphs, monohydrate and co-crystals with iodine: study from the energetic viewpoint, RSC Adv. 14 (2024) 29774, https://doi.org/10.1039/D4RA04368E.
[24] C.F. Macrae, I. Sovago, S.J. Cottrell, P.T.A. Galek, P. McCabe, E. Pidcock, M. Platings, G.P. Shields, J.S. Stevens, M. Towler, P.A. Wood, Mercury 4.0: from visualization to analysis, design and prediction, J. Appl. Crystallogr. 53 (2020) 226–235, https://doi.org/10.1107/S1600576719014092.
[25] S. Grimme, Semiempirical GGA-type density functional constructed with a long-range dispersion correction, J. Comput. Chem. 27 (2006) 1787, https://doi.org/10.1002/jcc.20495.
[26] S. Grimme, J. Antony, S. Ehrlich, H. Krieg, A consistent and accurate ab initio parametrization of density functional dispersion correction (DFT-D) for the 94 elements H–Pu, J. Chem. Phys. 132 (2010) 154104, https://doi.org/10.1063/1.3382344.
[27] S. Grimme, S. Ehrlich, L. Goerigk, Effect of the damping function in dispersion corrected density functional theory, J. Comput. Chem. 32 (2011) 1456, https://doi.org/10.1002/jcc.21759.
[28] A. Schäfer, H. Horn, R. Ahlrichs, Fully optimized contracted Gaussian basis sets for atoms Li to Kr, J. Chem. Phys. 97 (1992) 2571, https://doi.org/10.1063/1.463096.
[29] F. Weigend, R. Ahlrichs, Balanced basis sets of split valence, triple zeta valence and quadruple zeta valence quality for H to Rn: design and assessment of accuracy, Phys. Chem. Chem. Phys. 7 (2005) 3297, https://doi.org/10.1039/B508541A.
[30] S.F. Boys, F. Bernardi, The calculation of small molecular interactions by the differences of separate total energies. Some procedures with reduced errors, Mol. Phys. 19 (1970) 553, https://doi.org/10.1080/00268977000101561.
[31] L. Goerigk, S. Grimme, A thorough benchmark of density functional methods for general main group thermochemistry, kinetics, and noncovalent interactions, Phys. Chem. Chem. Phys. 13 (2011) 6670, https://doi.org/10.1039/C0CP02984J.
[32] F. Neese, Software update: the ORCA program system – version 5.0, Wiley interdiscip, Comput. Mol. Sci. 12 (2022) e1606, https://doi.org/10.1002/wcms.1606.
[33] F. Slamang, E.C. Hostena, R. Betz, 3-Iodoaniline, IUCrData 9 (2024) x241226, https://doi.org/10.1107/S2414314624012264.
[34] F. Kleemiss, O.V. Dolomanov, M. Bodensteiner, N. Peyerimhoff, M. Midgley, L. J. Bourhis, A. Genoni, L.A. Malaspina, D. Jayatilaka, J.L. Spencer, F. White, B. Grundkoetter-Stock, S. Steinhauer, D. Lentz, H. Puschmann, S. Grabowsky, Chem. Sci. 12 (2021) 1675–1692.

[35] L.J. Bourhis, O.V. Dolomanov, R.J. Gildea, J.A.K. Howard, H. Puschmann, Acta Crystallogr. A 71 (2015) 59–75.
[36] O.V. Dolomanov, L.J. Bourhis, R.J. Gildea, J.A.K. Howard, H. Puschmann, J. Appl. Crystallogr. 42 (2009) 339–341.
[37] A. Corozzi, B. Mennucci, R. Cammi, J. Tomasi, Structure versus solvent effects on nonlinear optical properties of push–pull systems: a quantum-mechanical study based on a polarizable continuum model, J. Phys. Chem. A 113 (2009) 14774–14784, https://doi.org/10.1021/jp904906n.
[38] O.V. Shishkin, I.S. Konovalova, R.I. Zubatyuk, G.V. Palamarchuk, S.V. Shishkina, A.V. Biitseva, I.V. Rudenko, V.A. Tkachuk, M.Y. Kornilov, O.V. Hordiyenko, J. Leszczynski, Remarkably strong polarization of amidine fragment in the crystals of 1-imino-1H-isoindol-3-amine, Struct. Chem. 24 (2013) 1089–1098, https://doi.org/10.1007/s11224-012-0131-y.
[39] P. Politzer, J.S. Murray, T. Clark, Halogen bonding and other σ-hole interactions: a perspective, Phys. Chem. Chem. Phys. 15 (2013) 11178, https://doi.org/10.1039/C3CP00054K.
[40] E.R.T. Tiekink, Supramolecular architectures sustained by delocalised C–I···π (arene) interactions in molecular crystals and the propensity of their formation, CrystEngComm 23 (2021) 904–928.
[41] Eds.E.R.T. Tiekink, J. Zukerman-Schpector (Eds.), The Importance of Pi-Interactions in Crystal Engineering: Frontiers in Crystal Engineering, John Wiley & Sons, 2012.
[42] S. Hu, Z. Zhou, Z. Xie, B. Robertson, A comparative study of crystallographic van der Waals radii, Z. Kristallogr. – Cryst. Mater. 229 (2014) 517, https://doi.org/10.1515/zkri-2014-172.
[43] V.G. Saraswatula, B.K. Saha, New. J. Chem. 38 (2014) 897–901.
[44] M.V. Chernysheva, M. Bulatova, X. Ding, M. Haukka, Cryst. Growth Des. 20 (2020) 7197–7210, https://doi.org/10.1021/acs.cgd.0c00866.